


Cite this: *RSC Adv.*, 2018, 8, 25636

Synthesis of switchable intelligent molecularly imprinted polymers with selective adsorption of ethyl carbamate and their application in electrochemical sensor analysis†

Ming Guo,^{*ab} Xinge Zhang,^{ab} Yilu Zheng^{ab} and Dinghai Huang ^{*c}

A cyclodextrin aldehyde based molecularly imprinted polymer with thermally responsive Diels–Alder (DA) linkages of grafted furan-type dienes was polymerized. The synthesized DA-MIP has dienophile characteristics and the specific absorption of ethyl carbamate (EC) can be switched on or off simply by thermal adjustment to 130 °C and 60 °C, respectively. The imprinting factors (α) of the MIP and rDA-MIP to EC were 6.2 and 5.0, and the selection factors (β) were 5.2 and 4.0, respectively. The restoration of the molecular target ratio was 88%, as determined by absorption and desorption experiments. The thermal restoration ratio, determined by thermal cycling experiments, was 78%. A new electrochemical sensor was prepared using the DA-MIP and its responsiveness for detecting trace amounts of EC was investigated. The results indicate that the electrode response has good affinity and excellent specific recognition performance for template molecular chemicals.

Received 21st May 2018

Accepted 2nd July 2018

DOI: 10.1039/c8ra04323j

rsc.li/rsc-advances

1 Introduction

Ethyl carbamate (EC) is a typical example of a carcinogenic carbamate compound, which has been found in fermented drinks such as wine and other alcoholic beverages.^{1–3} Since 2002, the World Health Organization has made EC a key monitoring substance. At present, the standards for limits on EC content in imported wines, spirits and other liquors have correspondingly set EC content as a critical technical factor in international trade.^{4,5} Therefore, rice wine related products will face testing challenges during trade, in which the detection of EC content is one of the critical factors.^{6–8}

In the literature, several methods have been developed for determining EC, including high performance liquid chromatography (HPLC), gas chromatography (GC), liquid chromatography-mass spectrometry (HPLC-MS-MS) and gas chromatography-mass spectrometry (GC-MS). These methods have major drawbacks as they make it very difficult to detect trace amounts of EC in high cost fermented drinks.^{9–11}

At the same time, traditional rice wine with its characteristics of high temperature decoction, low temperature brewing and being consumed at room temperature will be inconvenient for EC detection. Therefore, it is essential to develop technology with an online real-time measurement system to avoid the problems that require fixed temperatures to accurately reflect the content of EC.¹²

Molecular Imprinting Technology (MIT) is a form of biomimetic Molecular Recognition Technology which simulates the molecular recognition of antigens and antibodies in nature.^{13–15} Template molecules interact with functional monomers to produce stable polymers by intermolecular interactions that utilize the chemical cross-linking reaction. By eluting the template molecules, a molecular imprinted polymer (MIP) is produced which retains binding sites and holes^{16–20} that exactly match the size and shape of the original template, and such structures are like locks and keys. MIPs prepared by conventional methods exhibit high specific selectivity, strong stability and wide utilizations in chromatographic separation, solid phase extraction, simulated enzyme catalysis and membrane separation.^{21–25} At present, the preparation of intelligent molecular imprinting sensors for electrochemical sensing is an innovative frontier in MIP material science, and combining the specific recognition performance of MIPs with the detection sensitivity of electrochemical sensors has become an active field in new sensor research.

Using a covalent method, this work utilizes the thermal reversibility of the Diels–Alder reaction^{26–31} to prepare a novel kind of temperature-sensitive molecular imprinting polymer

^aDepartment of Chemistry, Zhejiang Agricultural & Forestry University, Hangzhou, Zhejiang, 311300, China. E-mail: guoming@zafu.edu.cn

^bNational Engineering and Technology Research Center of Wood-based Resources Comprehensive Utilization, Zhejiang Agricultural & Forestry University, Hangzhou, Zhejiang, 311300, China

^cDepartment of Polymer Material Science and Engineering, Institute of Advanced Polymer Materials, School of Materials Science and Engineering, Tianjin University, Tianjin 300350, China. E-mail: dhuang@tju.edu.cn

† Electronic supplementary information (ESI) available. See DOI: 10.1039/c8ra04323j



material and the specific imprinting absorption can be switched on or off by the incorporated thermally reversible Diels–Alder reaction. The present work is in accordance with the development trend of molecular imprinting technology, and also takes into account the existing difficulties in the enrichment of ethyl carbamate. Molecularly imprinted polymers that have the advantages of specific recognition, structure–activity reservation, temperature sensitivity and environmental stability are expected to play a critical role in EC detection assays, enrichment and efficient reduction. Hence, it is momentous to carry out research on this new intelligent molecularly imprinted polymer of EC.

2 Experimental section

2.1 Reagents and chemicals

Triethylamine, Na₂CO₃, Al₂O₃, anhydrous CaCl₂, sodium ethoxide, KH-560, 2-iodoyl benzoic acid (IBX), *N,N*-dimethylformamide (DMF) and furoyl chloride were purchased from Energy Chemical. Silica gel, urethane, methyl carbamate, *tert*-butyl carbamate and maleimide were obtained from Saun Chemistry. Methylbenzene, acetone, diethyl ether, dimethyl sulfoxide, graphite powder, potassium iron(III) cyanide, monometallic sodium orthophosphate and disodium hydrogen phosphate were purchased from Hangzhou Dafang Chemical Reagent Factory. All chemicals were of analytical grade. All aqueous solutions were prepared with distilled water (18.2 MΩ, Millipore, Bedford, MA).

2.2 Apparatus

The infrared absorption spectra of coatings were obtained between 400 and 4000 cm^{−1} using a FTIR spectrophotometer (Japan Shimadzu company/IR Prestige-21).

Samples of MIP and DA-MIP were measured using cross-polarization/magic angle spinning (CP/MAS) to obtain ¹³C NMR spectra on an AVANCEII/400 MHz nuclear magnetic resonance spectrometer. The 4.88 Hz resolution ¹³C CP/MAS NMR spectra were obtained using a magic angle spin speed of 3.8 MHz and an observation frequency of 75 MHz, with 696 cumulative scans and 8192 acquired data-points. Amino acetic acid was used as a reference substance for the chemical shifts.

Morphology analysis was conducted using a Scanning Electron Microscope SSX-550 (Shimadzu, Japan) and samples were sputter-coated with gold using an SS-550-IC type sputtering device.

Thermo Gravimetric Analysis (TGA) was carried out using a TA Q500 Thermo Gravimetric Analyzer under a N₂ flow of 60 mL min^{−1} and was heated from 25 °C to 700 °C at a constant heating rate of 10 °C min^{−1}.

Samples of the DA-MIP, rDA-MIP and MIP were analyzed using differential scanning calorimetry (DSC, DSC200F3, Netzsch, Germany). The conditions of the DSC measurement were as follows: sample mass: 3–5 mg; heating rate: 10 °C min^{−1}; and nitrogen atmosphere (flow rate: 60 mL min^{−1}).

The HPLC (Agilent-1200, Keysight, China) system consisted of an Agilent HC-C₁₈ column and was performed at 30 °C. The mobile phase was acetonitrile : water = 80 : 20 (4 volume ratio).

The flow rate was maintained at 0.5 mL min^{−1} and 10 μL injections.

Electrochemical and cyclic voltammetric (CV) measurements were performed using an Electrochemical Workstation (Shanghai Chenhua Instruments Co., Chinese).

2.3 Synthesis and characterization of the DA-MIP

Details of the synthesis and characterization of the MIP and DA-MIP materials is available in the ESI, S1.†

2.4 HPLC analysis

The HPLC (Agilent-1200, Keysight, China) system consisted of an Agilent HC-C₁₈ column. HPLC chromatography was performed at 30 °C. The mobile phase was a mixture of acetonitrile and water with an 80 : 20 volume ratio. The flow rate was maintained at 0.5 mL min^{−1} and 10 μL injections.

Methyl carbamate (MC), ethyl carbamate (EC) and *tert*-butyl carbamate (BC) (0.1, 0.2, 0.4, 0.6, 0.8 and 1.0 mg L^{−1}) were prepared by diluting the solute in methanol. To obtain a standard curve, 10 μL of each solution was injected into the HPLC system and the area under the curve (AUC) for each peak was plotted *versus* the standard sample concentration.

2.4.1 High performance liquid chromatography detection for template molecular concentration. The template molecular (MIP, DA-MIP, NMIP) solution was freshly prepared by transferring 20 mg of template molecule, accurately weighed, to a 10 mL centrifuge tube (5 copies per sample) and methanol/EC was added to each sample. After mixing for 24 h and centrifuging, the upper layer was filtered through a 0.22 μm Millipore membrane filter and analyzed using HPLC.

For this assay, 0.02 g of MIP, DA-MIP, rDA-MIP and NMIP were accurately weighed and dissolved in methanol (5 mL) which had different concentrations of EC, BC and MC, respectively, before being added to a centrifuge tube. After mixing for 24 h, each sample was centrifuged. Then, the upper layer was transferred to a new tube and each concentration was injected into the HPLC system. All determinations were conducted in triplicate.

The amount of absorption can be written as follows:³²

$$Q = \frac{(C_0 - C_e)V}{W} \quad (1)$$

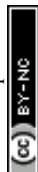
Q – absorption capacity (mmol L^{−1}); *C*₀ and *C*_e represent the initial and final concentrations of the substrate (mmol L^{−1}), respectively; *W* – mass of polymer (g); and *V* – absorption volume (mL).

Consequently, the imprinting factor, *α*, and selection factor, *β*, can be written as follows:³³

$$\alpha = \frac{Q_{\text{MIP}}}{Q_{\text{NMIP}}} \quad (2)$$

$$\beta = \frac{Q_{\text{MIP}} - Q_{\text{NMIP}}}{Q_{\text{NMIP}}} \quad (3)$$

where *Q*_{MIP} is the absorption amount of the molecularly imprinted polymers on the substrates and *Q*_{NMIP} is the



absorption amount of the no-treatment control group on the substrates.

2.5 Preparation and performance tests of the electrochemical sensor

50 mg of *n*-eicosane was put into a porcelain crucible, with a 45–50 °C water bath, mechanical stirring and heated to melt, then graphite powder (10 mg) and the MIP (10 mg) were added. After stirring, the mixture was filled into a polyvinyl chloride (PVC) tube with a diameter of 3 mm and finally, a graphite electrode (MIP-GE) was obtained. The MIP-GE electrode was polished with 0.3 and 0.05 μm Al_2O_3 and ultrasonicated in secondary water, anhydrous ethanol, and secondary water again (5 min per time), then dried at room temperature. DA-MIP-GEs, rDA-MIP-GEs, NMIP-GEs and bare electrodes (bare-GEs without any molecularly imprinted polymer) were prepared using the same procedure as described above.

Cyclic voltammetric (CV) measurements were recorded by applying a potential from -0.2 V to $+0.6$ V in 5 mmol L^{-1} of $\text{K}_3\text{Fe}(\text{CN})_6$, 0.1 mol L^{-1} KCl, and from 0.0 V to $+0.8$ V with a potential frequency of $0.01\text{--}1 \times 10^5$ Hz and an amplitude of 5 mV at a scan rate of 0.1 V s^{-1} .

The detection performance of the EC modified electrode was investigated by using differential pulse voltammetry in 0.01 mol L^{-1} PBS ($\text{pH} = 7$) to obtain the peak current I_0 of the MIP-II-GE; the MIP-II-GE was immersed in PBS solution at concentrations of $0.1, 0.2, 0.5, 1, 1.5, 2 \mu\text{mol L}^{-1}$. The peak current of the MIP-II-GE was obtained using DPV. Using eqn (4),³⁴ the EC sensor imprinting efficiency ($I\%$) can be calculated.

$$I\% = \frac{I_0 - I_1}{I_0} \times 100\% \quad (4)$$

The response of the electrode to EC can be measured by repeating the above operation.

3 Results and discussion

3.1 Synthesis and reaction mechanism of production

The synthesis of the imprinting polymer was carried out as follows. First, a silane coupling agent was chemically grafted onto the surface of silica gel. Then, IBX oxidized hydroxyl groups of C2 in cyclodextrin to obtain a cyclodextrin aldehyde. Finally, the furan ring was grafted in the 6th position of the cyclodextrin aldehyde to obtain DA-MIP (see ESI Fig. S1†).

Imprinting ethyl carbamate was synthesized based on the Schiff base reaction and epoxy chloropropane was crosslinked with β -cyclodextrin. After the template was eluted, the MIP was obtained. The furan-ring functioned MIP and maleimide were reacted to block the eluted pores by the Diels–Alder (DA) reaction, to obtain the DA-MIP without imprinting function.^{26–31} The MIP and maleimide were filled with the eluted pores by Diels–Alder (DA) reaction to prepare a DA-MIP with weak imprinting function, and the DA-MIP can be used as a raw material for preparing the imprinted polymer rDA-MIP. The synthetic route is shown in Fig. 1.

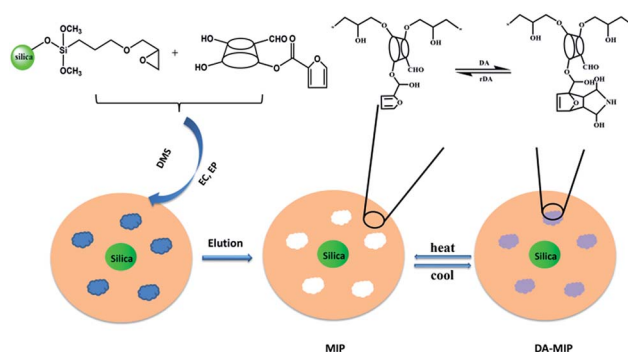


Fig. 1 The synthetic route of DA-MIP.

3.2 Characterization of the raw material, intermediates and DA-MIP

3.2.1 FT-IR spectra of the raw material, intermediates and DA-MIP. FT-IR spectra of the raw material, intermediates and DA-MIP are shown in Fig. 2 and table S1 (see ESI†).

For silica gel, the peaks at 3442 cm^{-1} and 799 cm^{-1} correspond to the $-\text{OH}$ stretching vibration of hygroscopic water and $\text{Si}(\text{OH})$ stretching vibrations, respectively. It can be seen that the peaks at 1630 cm^{-1} and 589 cm^{-1} are due to $-\text{OH}$ and $\text{Si}-\text{O}$ bending vibrations, respectively. The peak at 1150 cm^{-1} can be ascribed to $\text{Si}-\text{O}-\text{Si}$ asymmetrical stretching vibrations.³⁵ The peak at 982 cm^{-1} is due to $\text{Si}-\text{OH}$ hydroxyl groups associated with $-\text{OH}$ variable angular vibrations. All of these peaks are almost at the same positions when compared with the silica gel-KH-560.³⁶

In the FT-IR spectra of the silica gel-KH-560, the peaks at 2990 cm^{-1} and 1050 cm^{-1} are due to methyl $\text{C}-\text{H}$ and $\text{C}-\text{O}-\text{C}$ stretching, respectively. In addition, the peak observed at 922 cm^{-1} was ascribed to an epoxy group.

For the MIP, the peaks at 3670 cm^{-1} and 1722 cm^{-1} correspond to $-\text{OH}$ and $\text{C}=\text{O}$ stretching, respectively. The two peaks at 1210 cm^{-1} and 1076 cm^{-1} correspond to furan ring $\text{C}-\text{O}-\text{C}$ symmetric stretching vibrations and asymmetric stretching vibrations, respectively. The peak at 2160 cm^{-1} is ascribed to the furan ring which contains a system of conjugated double bonds. The peak at 1510 cm^{-1} is attributed to the carbon

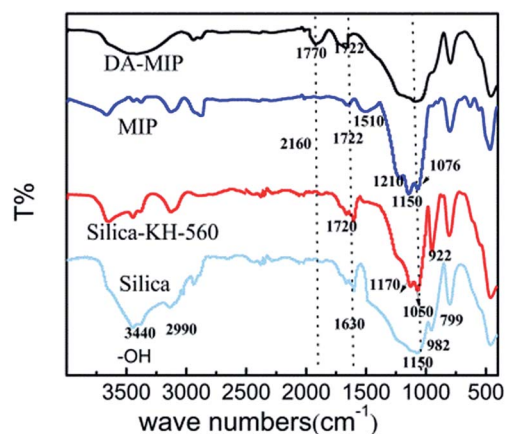


Fig. 2 FT-IR spectra of the raw material, intermediates and DA-MIP.



skeleton stretching of the furan ring. Meanwhile, the characteristic absorption peak of the epoxy group (922 cm^{-1}) disappeared, indicating that the furan ring was grafted onto the surface of the silica gel successfully.

For the DA-MIP, three peaks disappeared at 1210 cm^{-1} , 1076 cm^{-1} and 2160 cm^{-1} , due to the DA reaction. The 1210 cm^{-1} and 1076 cm^{-1} peaks corresponding to furan ring stretching vibrations and C–O–C stretching vibrations, respectively, disappeared. Also due to the DA reaction, the peak at 2160 cm^{-1} corresponding to conjugated double bonds in the furan ring disappeared. Meanwhile, a peak at 1770 cm^{-1} ascribed as the characteristic peak of the DA bond³⁷ appeared, while other bone structures in the silica gel were still retained.

The IR spectra of β -cyclodextrin and its derivatives are shown in Fig. S2 (see ESI†) and these results indicate that β -CD-CHO and furan- β -CD-CHO were successfully synthesized (more details in the discussion, see ESI S2†).

3.2.2 The ^{13}C -NMR characterization of MIP and DA-MIP. Nuclear magnetic spectra are shown in Fig. S3 (see ESI†) and the main peaks are shown in Table S2 (see ESI†).

The measured ^{13}C CP/MAS NMR spectrum of the MIP sample is depicted in Fig. S3a.† Besides the signals related to the carbons of β -cyclodextrin and linear carbon atoms, additional peaks were observed in the ^{13}C CP/MAS NMR spectrum (MIP sample). The signals near 110.4 ppm (C9), 116.6 ppm (C2), 141.1 ppm (C10) and 145.5 ppm (C11) indicate the presence of the furan ring.³⁸ The peak at 157.3 ppm is associated with the skeletal displacement of the carbon atom on the ester bond.

To prove the success of the DA reaction, the ^{13}C CP/MAS NMR spectrum of DA-MIP was obtained. The ^{13}C CP/MAS NMR spectrum of DA-MIP (see ESI Fig. S3b†) has similar features to that of MIP and signals related to the carbons of β -cyclodextrin and linear carbon atoms can be found in both of the two samples. In comparison to the spectrum of the MIP sample, the peaks of DA-MIP can be seen to have some differences. A signal near 90 ppm (C8) appeared and chemical shifts of the carbonyl group (near 33.0 ppm) are broadened. Chemical shifts near 110.4 ppm (C9) and 141.1 ppm (C10) indicating the presence of the furan ring disappeared and the DA bond appears on the C9, C10 carbon skeleton shifts at 140.0 ppm . In addition, carbonyl group peaks near 169.6 ppm also appear in the spectrum of the DA-MIP sample, revealing that maleimide is involved in the reaction. These results unambiguously indicate the success of the DA reaction in DA-MIP.

3.2.3 Scanning electron microscopy. A morphological study was carried out using a scanning electron microscope (SEM) to observe changes on the surface and within the microstructure of silica gel, before and after the chemical reaction.

Fig. 3a shows that the surface of the initial silica gel is uniform, delicate and dense. Fig. 3b displays SEM images of the MIP, which shows surface modification with pores and the average pore size is much larger. This revealed that MIPs contain cavities after the elution of template molecules. A more uniform surface morphology with few pores is observed in the DA-MIP (see Fig. 3c), which indicates that the retained pores after elution are repaired in a large area. Comparing Fig. 3c with Fig. 3d showed that the surface morphology of the rDA-MIP

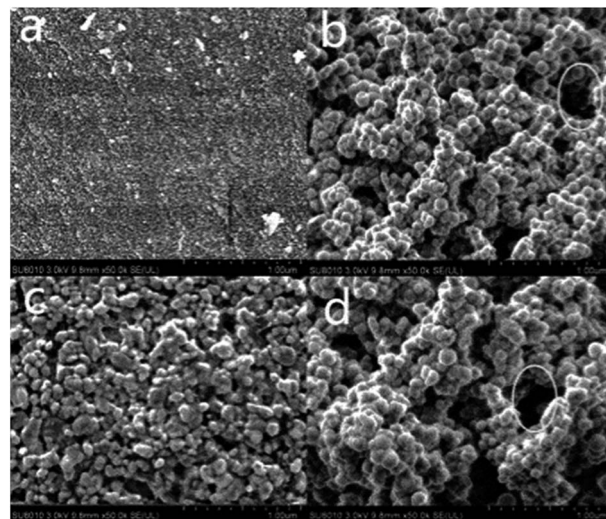


Fig. 3 SEM images of (a) silica gel; (b) MIP; (c) DA-MIP; (d) rDA-MIP.

became loose and had a relatively larger average pore size than that of DA-MIP.³⁹

These results revealed that the imprinted cavities were exposed due to the rupture of a DA bond after the heating of the DA-MIP and indicated the formation of a rDA-MIP.

3.3 Thermal properties of the raw materials, intermediate products and DA-MIP

3.3.1 Thermogravimetric curves. The thermogravimetric curves for the thermal degradation of samples are shown in Fig. S4 (see ESI†). There is no significant difference between the MIP and the DA-MIP and the total weight loss of the two samples is 19–23% up to $600\text{ }^{\circ}\text{C}$, which indicates that the synthesized polymers have good thermal properties (more details in the discussion, see ESI S3†).

3.3.2 Study of the thermal properties by DSC. Fig. 4 shows the DSC curves of MIPs, DA-MIPs, and rDA-MIPs. The DA-MIP exhibited an endothermic peak at about $130\text{ }^{\circ}\text{C}$, which implied the fracture of the Diels–Alder adduct bonds.^{40–42} There was no endothermic peak in the whole temperature range for the MIP because the DA reaction is absent in the MIPs. After the reverse DA reaction, the DA bond breaks, and no endothermic peaks appear in the measured temperature range, indicating the presence of DA bonds in DA-molecularly imprinted polymers. It should be noted that Froidevaux *et al.* found that, compared to the DSC method, the ^1H NMR method can detect Diels–Alder or retro-Diels–Alder reaction kinetics and temperatures more precisely.⁴⁰

3.4 Study of the specific absorption and recognition performance of DA-molecularly imprinted polymers for ethyl carbamate

3.4.1 Isothermal static absorption curve. The amount of absorption was calculated according to eqn (1), and the isothermal absorption curve is shown in Fig. 5.

As shown in Fig. 5, for the MIP and rDA-MIP, EC uptake increased sharply in the initial stage and then became slower, finally reaching an equilibrium platform. This phenomenon



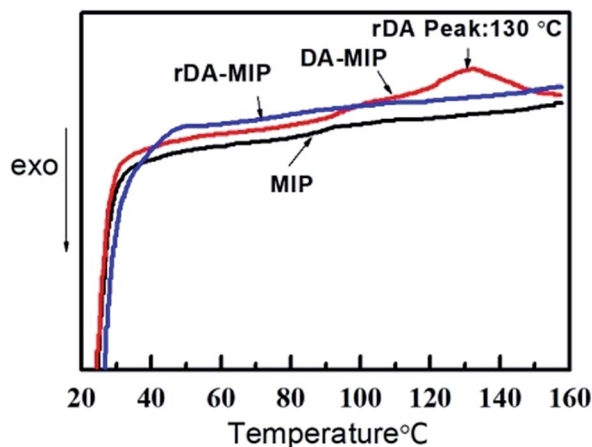


Fig. 4 The DSC heating traces of the DA-MIP, rDA-MIP and MIP, respectively.

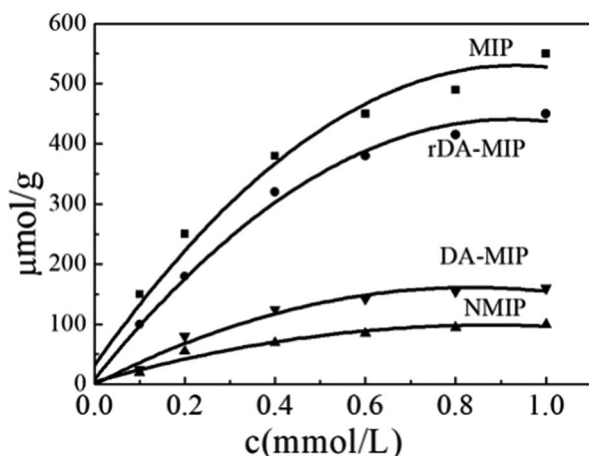


Fig. 5 The absorption isotherm of the MIP, NMIP, rDA-MIP and DA-MIP on EC.

may be due to the fact that, initially, all active sites on the MIP composite surface were vacant. Compared with the MIP, the absorption trend of the rDA-MIP is almost the same, but the absorption capacity is reduced. This is due to the decrease in absorption sites by the reverse DA reaction. The absorption capacity of both the DA-MIP and NMIP was significantly lower than those of the MIP and rDA-MIP and as we know, the absorption capacity depends on the spatial structure and binding sites. The NMIP does not have the space structure and binding site of the DA-NMIP, making it lose the ability to bind to template molecules due to the DA reaction.

3.4.2 Specific absorption and molecular recognition. Fig. 6 shows absorption quantities. It can be observed that by using the MIP as the adsorbent, the absorption of EC is much larger than that of MC and BC. The MIP presents a specific affinity of absorption for the template (*i.e.* EC). Apparently, the specific imprint within MIP plays a critical role in specific absorption. When using rDA-MIPs as adsorbent, there is also a remarkable difference when comparing EC, MC and BC. Its absorption

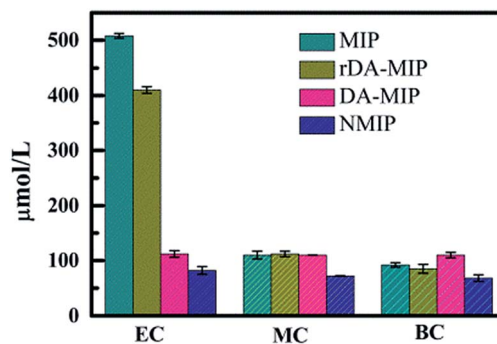


Fig. 6 The absorption quantities of the MIP, NMIP, rDA-MIP and DA-MIP on EC, MC and BC.

capacity for EC is only slightly lower than that of the MIP. As discussed in the previous section, the rDA-MIP recognition capacity recovered incompletely compared with the molecular imprinted polymer because of the residues of part DA bonds by the DA reverse reaction. In comparison, the DA-MIP showed a very poor absorption capacity for EC. This result showed that by introducing the Diels–Alder reaction into the MIP material, its molecular imprint specific absorption can easily be switched on or off using special temperatures.

It can be seen from Table 1 that the Q_{MIP} value of EC is obviously greater than those of its analogues. It is found that by using the MIP as an adsorbent, the absorption of EC is much larger than that of MC and BC. The MIP presents a specific affinity of adsorption of the template (*i.e.* EC). Apparently, the specific imprint within the MIP plays a critical role in specific adsorption. When using rDA-MIP as an adsorbent, there is also a remarkable difference when comparing EC, MC and BC.

The kinetic information obtained from adsorption experiments indicates that the MIP and rDA-MIP have good specific adsorption properties. At present the kinetics of the binding are still not very clear, and the results suggest a need for further investigation into this phenomenon.

Table 1 The adsorption quantities of the MIP, NMIP, rDA-MIP and DA-MIP on EC, MC and BC^a

Parameter	EC	MC	BC
Q_{MIP} ($\mu\text{mol L}^{-1}$)	508	110	82
$Q_{\text{rDA-MIP}}$ ($\mu\text{mol L}^{-1}$)	410	112	85
$Q_{\text{DA-MIP}}$ ($\mu\text{mol L}^{-1}$)	112	110	110
Q_{NMIP} ($\mu\text{mol L}^{-1}$)	82	72	68
α_{MIP}	6.20	1.53	1.21
β_{MIP}	5.20	0.53	0.21
$\alpha_{\text{rDA-MIP}}$	5.00	1.56	0.21
$\beta_{\text{rDA-MIP}}$	4.00	0.56	0.21
$\alpha_{\text{DA-MIP}}$	1.37	1.53	1.62
$\beta_{\text{DA-MIP}}$	0.37	0.53	0.62

^a Where Q_{MIP} ($\mu\text{mol L}^{-1}$) is the adsorption capacity of the template molecules or analogues on the imprinted polymer; Q_{NMIP} ($\mu\text{mol L}^{-1}$) is the adsorption capacity of the template molecules or analogues on the non imprinted polymers; α_{MIP} is the imprinting factor of the template molecules; α_{ana} is the imprinting factor of the analogues, such as MC and BC; and $\alpha = Q_{\text{MIP}}/Q_{\text{NMIP}}$.



More details about the absorption standard curve, kinetics, and the absorption model and discussions can be found in the ESI, S4.†

3.5 Performance research on the recyclability of the rDA-MIP

After elution, the MIP was soluted in EC methanol at a constant temperature and shaken for 24 h. In a limited time, the absorption–stripping ability of the MIP was re-run 5 times^{32,43,44} and the restoration ratio is illustrated in Fig. S10 (see ESI†). The amount of absorption was measured and compared with that of the MIP by repeating the DA reaction and reverse DA reaction according to the method described in Section 2.2.

It can be seen from Fig. S10† that there was around a 3% drop in absorption capacity after each recycling procedure. The absorption–stripping ability of the MIP was tested 5 times in the experiment and it was found that the recovery rate was still maintained at 88%. This revealed the good renewable absorption performance of the MIP and a renewability test also revealed that the rDA-MIP is quite stable. It can be observed from Fig. 7 that, compared with the MIP, the absorption capacity of rDA1 decreased to 85% of the original and after three cycles, the rDA3 absorption decreased to 78% which indicated that the rDA-MIP still has good specific absorption performance after several recycling procedures. There is no significant change in absorption capacity between DA1, DA2 and DA3. That indicates that although the DA reaction may affect the absorption performance of the rDA-MIP in some sense, the thermal cycle has little effect on the DA-MIP.

3.6 Detection sensitivity of the molecularly imprinted sensor

3.6.1 Scanning results of different electrodes using cyclic voltammetry. Fig. 8 shows the CV responses of different electrodes. The voltammograms are stable in subsequent cycles with an anodic-to-cathodic peak current ratio of 1.0. This indicates the chemical reversibility of the process.⁴⁵ The maximum peak of ion current was probed in the MIP-GE electrode due to the formation of pores in the MIP and the active sites of absorption on the electrode surface are enhanced. The peak ion current of the DA-MIP-GE electrode decreased significantly, because the imprinting pores were filled-up by the DA reaction. In comparison, the peak current of the rDA-MIP-GE is just

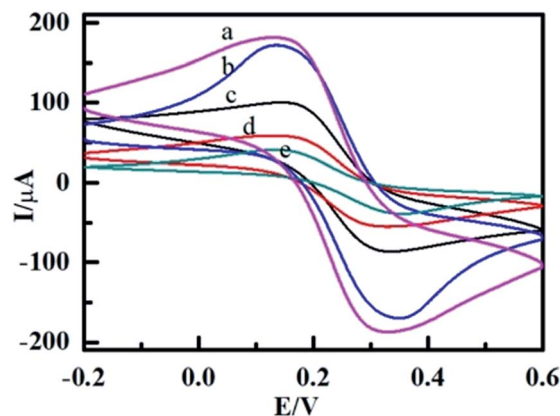


Fig. 8 Cyclic voltammogram responses for different electrodes. (a) MIP-GE; (b) rDA-MIP-GE; (c) DA-MIP-GE; (d) NMIP-GE; (e) bare-GE.

slightly lower than that of the MIP-GE. This indicates that the inverse DA reaction basically restores the original pore structure of the MIP. The lowest peak current was that of the bare-GE, which has a smooth surface, thereby hindering the redox reaction of $[\text{Fe}(\text{CN})_6]^{4-/3-}$.

Since NMIP does not add template molecules, there will be no imprinted holes and active sites and the surface structure of the prepared electrode has no obvious difference compared to that of the bare-GE. Therefore, the difference between the NMIP-GE and bare-GE in terms of the peak current is not significant.

More discussion about the electrochemical results can be seen in the ESI, S5.1 to S5.3.†

3.6.2 Differential pulse voltammetry (DPV). The absorption performance of EC was analyzed according to the Experimental section, and the results are shown in Fig. 9.

Fig. 9A shows that the peak current increased significantly with increasing concentrations of EC. The response sensibility of different electrodes for constant concentrations of EC is illustrated in Fig. 9B. MIP-GE (curve a in Fig. 9B) has the highest response current to EC and this result is in accordance with the characteristics of the specific absorption of MIP to EC. The response of the DA-MIP-GE (curve c) to EC was significantly reduced. This phenomena demonstrated that the DA reaction which reduced the recognition sites hinder the mass transfer process. Although when compared with the MIP-GE the current intensity was slightly reduced, the response current of the rDA-MIP-GE (curve b) to EC restoration rate is still as high as 92%. NMIP-GE (curve d) has the lowest response current because the lack of specific binding sites makes the absorption of EC an intermolecular indiscriminative absorption process. The significant differences in the detection of DPV for different electrodes indicates the specific absorption performance and its excellent switchability by the Diels–Alder reaction of the rDA-MIP. More details regarding the electrochemical sensor performance can be seen in the ESI, S5.4 to S5.5.†

It should be noted that all of the absorption and electrochemical experiments are conducted in aqueous solution at ambient temperatures. It remains unclear whether the thermally switchable molecular recognition function can be directly

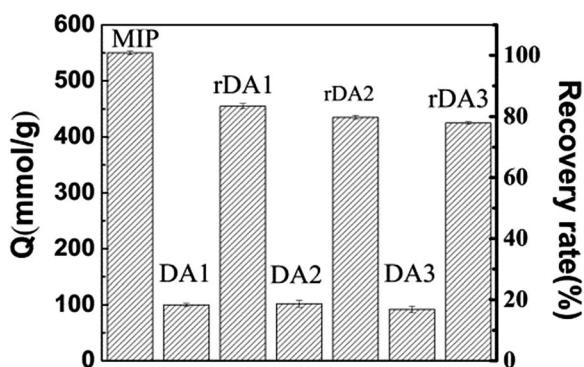


Fig. 7 Absorption of three cycle products for the rDA-MIP.



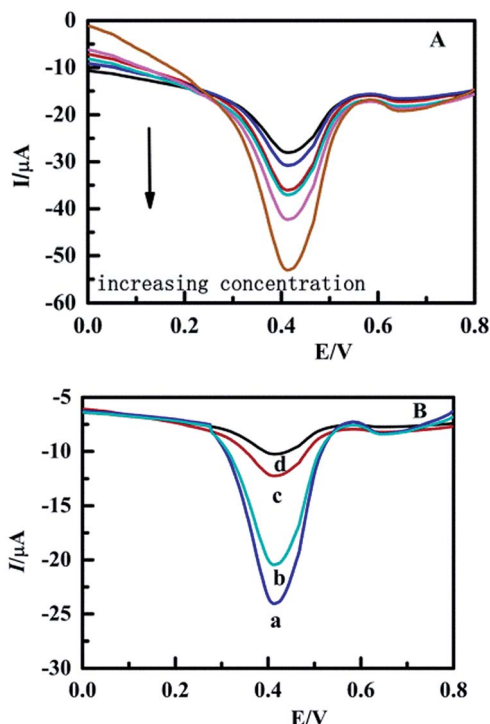


Fig. 9 The DPV for the MIP-GE modified with different concentrations of EC and the DPV of different electrodes for EC. (a) MIP-GE; (b) rDA-MIP-GE; (c) DA-MIP-GE; (d) NMIP-GE.

in situ turned on or off at increased temperatures, and further investigation is required to understand this.

4 Conclusions

In this study, the Diels–Alder (DA) reaction is applied in the synthesis of MIPs by a reversible chemical reaction between the special molecular structures in the system, which gives the synthesized novel MIP the characteristics of thermally switchable performance, and intelligent thermally reversible molecularly imprinted performance. The MIPs were synthesized and characterized using FT-IR, ^{13}C NMR and SEM, which indicated that DA bonds were successfully introduced into the two target products to form two novel imprinted polymers with thermally reversible characteristics. The performance test shows that the product has better thermal performance. The absorption experiments show that the products synthesized materials have good specific absorption properties and the recovery rate remains at 88% after recycling five times. Scatchard model analysis and Langmuir model simulation were used to compare the binding characteristics of the MIP and its DA product binding sites, and both of them show better binding properties than those of 5 electrodes which were prepared and a sensor that was constructed. CV and FRA detection confirmed that the target electrode was successfully prepared. The DPV electrode showed that the DA-MIP and rDA-MIP had better absorption properties for EC. The relation between the response current and the absorption time was analyzed. It was shown that the MIP-GE and rDA-MIP-GE had the same current response trend

and the enrichment time was short. Absorption specificity is also good. The present experimental results provide new information towards the possible development of intelligent materials. This new synthesis method can be used in the field of solid phase extraction, thin layer chromatography and so on.

Conflicts of interest

There are no conflicts to declare.

Acknowledgements

This work was financially supported by the Zhejiang Provincial Natural Science Foundation of China (No. LY18B070003), the Open Fund of Zhejiang Bamboo Resources and Efficient Usage of “2011” Collaborative Innovation Center (2017ZZY2-09), and the Project of Zhejiang Provincial Key Laboratory of Chemical Utilization of Forestry Biomass, The Scientific and Technological Cooperation Project of People’s Government of Zhejiang Province-Chinese Academy of Forestry (2015SY11).

Notes and references

- 1 X. W. Guo, Y. Z. Li, J. Guo, Q. Wang and S. Y. Huang, Reduced production of ethyl carbamate for wine fermentation by deleting *CAR1* in *Saccharomyces cerevisiae*, *J. Ind. Microbiol. Biotechnol.*, 2016, **43**, 671–679.
- 2 D. Ryu, B. Choi, N. Kim and E. Koh, Validation of analytical methods for ethyl carbamate in nine food matrices, *Food Chem.*, 2016, **211**, 770–775.
- 3 J. Kowalska and A. Jezewska, Studies on an efficient method for determining ethyl carbamate in the workplace air, *Int. J. Environ. Sci. Technol.*, 2016, **13**, 1833–1838.
- 4 G. H. Li, Q. D. Zhong, D. B. Wang, *et al.*, Determination and Formation of Ethyl Carbamate in Chinese spirits, *Food Control*, 2015, **56**, 169–176.
- 5 Z. Huang, X. D. Pan, P. G. Wu, *et al.*, Validation (in-house and laboratory) of the quantification method for ethyl carbamate in alcoholic beverages and soy sauce by GC-MS, *Food Chem.*, 2013, **141**, 4161–4165.
- 6 D. Yang, H. Zhou, Y. Ying, *et al.*, Surface-enhanced Raman scattering for quantitative detection of ethyl carbamate in alcoholic beverages, *Anal. Bioanal. Chem.*, 2013, **405**, 9419–9425.
- 7 L. Luo, Y. Song, C. Z. Zhu, S. F. Fu, *et al.*, Fluorescent silicon nanoparticles-based ratiometric fluorescence immunoassay for sensitive detection of ethyl carbamate in red wine, *Sens. Actuators, B*, 2018, **255**, 2742–2749.
- 8 Z. Z. Wu, E. B. Xu, J. P. Li, J. Long, A. Q. Jiao and Z. Y. Jin, Highly sensitive determination of ethyl carbamate in alcoholic beverages by surface-enhanced Raman spectroscopy combined with a molecular imprinting polymer, *RSC Adv.*, 2016, **6**, 109442–109452.
- 9 H. S. Lim and K. G. Lee, Development and validation of analytical methods for ethyl carbamate in various fermented foods, *Food Chem.*, 2011, **126**, 1373–1379.



- 10 Z. Fu, L. Yang, L. Ma, X. Liu and J. Li, Occurrence of ethyl carbamate in three types of Chinese wines and its possible reasons, *Food Sci. Biotechnol.*, 2016, **25**, 949–953.
- 11 Y. W. Chin, W. K. Kang, H. W. Jang, T. L. Turner and H. J. Kim, *CAR1* deletion by CRISPR/Cas9 reduces formation of ethyl carbamate from ethanol fermentation by *Saccharomyces cerevisiae*, *J. Ind. Microbiol. Biotechnol.*, 2016, **43**, 1517–1525.
- 12 L. Luo, H. T. Lei, J. Y. Yang, G. L. Liu and Y. M. Sun, Development of an indirect ELISA for the determination of ethyl carbamate in Chinese rice wine, *Anal. Chim. Acta*, 2017, **950**, 162–169.
- 13 H. S. Byun, Y. N. Youn, Y. H. Yun and S. D. Yoon, Selective separation of aspirin using molecularly imprinted polymers, *Sep. Purif. Technol.*, 2010, **74**, 144–153.
- 14 C. Alexander, H. S. Andersson, L. Andersson, R. J. Ansell and N. Kirsch, Molecular imprinting science and technology: a survey of the literature for the years up to and including, 2003, *J. Mol. Recognit.*, 2006, **19**, 106–180.
- 15 G. Raquel, M. D. R. G. da Silva and M. J. Cabrita, “On-off” switchable tool for food sample preparation: merging molecularly imprinting technology with stimuli-responsive blocks. Current status, challenges and highlighted applications, *Talanta*, 2018, **176**, 479–484.
- 16 A. M. Shrivastav, S. K. Mishra and B. D. Gupta, Fiber optic SPR sensor for the detection of melamine using molecular imprinting, *Sens. Actuators, B*, 2015, **212**, 404–410.
- 17 K. Zhao, T. Chen, B. Lin, W. Cui and B. Kan, Absorption and recognition of protein molecular imprinted calcium alginate/polyacrylamide hydrogel film with good regeneration performance and high toughness, *React. Funct. Polym.*, 2015, **87**, 7–14.
- 18 A. Lakka and A. Tsakal, Molecular Imprinting of Tri-O-Acetyladenosine for the Synthetic Imitation of an ATP-Binding Cleft in Protein Kinases, *Chempluschem*, 2013, **78**, 808–815.
- 19 D. A. Spivak and J. Campbell, Systematic study of steric and spatial contributions to molecular recognition by non-covalent imprinted polymers, *Analyst*, 2001, **126**, 793–797.
- 20 L. Ye, Molecularly imprinted polymers with multi-functionality, *Anal. Bioanal. Chem.*, 2016, **408**, 1727–1733.
- 21 A. L. Hillberg, K. R. Brain and C. J. Allender, Molecular imprinted polymer sensors: implications for therapeutics, *Adv. Drug Delivery Rev.*, 2005, **57**, 1875–1889.
- 22 X. L. Wei and S. M. Husson, Surface-Grafted, Molecularly Imprinted Polymers Grown from Silica Gel for Chromatographic Separations, *Ind. Eng. Chem. Res.*, 2007, **46**, 2117–2124.
- 23 R. Panahi, E. Vasheghani-Farahani and S. A. Shojaosadati, Separation of l-lysine from dilute aqueous solution using molecular imprinting technique, *Biochem. Eng. J.*, 2007, **35**, 352–356.
- 24 K. Farrington, E. Magner and F. Regan, Predicting the performance of molecularly imprinted polymers: selective extraction of caffeine by molecularly imprinted solid phase extraction, *Anal. Chim. Acta*, 2006, **566**, 60–68.
- 25 X. Qi, S. Gao, G. Ding and A. N. Tang, Synthesis of surface Cr(VI)-imprinted magnetic nanoparticles for selective dispersive solid-phase extraction and determination of Cr(VI) in water samples, *Talanta*, 2017, **162**, 345–353.
- 26 R. Gheneim, C. Perez-Berumen and A. Gandini, Diels–Alder Reactions with Novel Polymeric Dienes and Dienophiles: Synthesis of Reversibly Cross-Linked Elastomers, *Macromolecules*, 2002, **35**, 7246–7253.
- 27 A. Gandini, The furan/maleimide Diels–Alder reaction: a versatile click–unclick tool in macromolecular synthesis, *Prog. Polym. Sci.*, 2013, **38**, 1–29.
- 28 D. N. Amato, G. A. Strange, J. P. Swanson, A. D. Chavez, S. E. Roy, K. L. Vamey, C. A. Machado, D. V. Amato and P. J. Costanzo, Synthesis and evaluation of thermally-responsive coatings based upon Diels–Alder chemistry and renewable materials, *Polym. Chem.*, 2014, **5**, 69–76.
- 29 R. Araya-Hermosilla, G. Fortunato, A. Pucci, P. Raffa, L. Polgar, A. A. Broekhuis, P. Pourhossein, G. M. R. Lima, M. Beljaars and F. Picchioni, Thermally reversible rubber-toughened thermoset networks via Diels–Alder chemistry, *Eur. Polym. J.*, 2016, **74**, 229–240.
- 30 L. M. Polgar, E. Hagting, W. J. Koek, F. Picchioni and M. van Duin, Thermoreversible Cross-Linking of Furan-Containing Ethylene/Vinyl Acetate Rubber with Bismaleimide, *Polymers*, 2017, **9**, 81.
- 31 J. W. Kim, D. H. Lee, H. J. Jeon, S. I. Jang, H. M. Cho and Y. Kim, Recyclable thermosetting thermal pad using silicone-based polyurethane crosslinked by Diels–Alder adduct, *Appl. Surf. Sci.*, 2018, **429**, 128–133.
- 32 L. Zhou, Q. Yu, Y. Cui, F. Xie, W. J. Li, Y. W. Li and M. F. Chen, Adsorption properties of activated carbon from reed with a high adsorption capacity, *Ecol. Eng.*, 2017, **102**, 443–450.
- 33 Y. Liu, X. Hu, Z. Liu, M. J. Meng, J. M. Pan, *et al.*, A novel dual temperature responsive mesoporous imprinted polymer for Cd(II) adsorption and temperature switchable controlled separation and regeneration, *Chem. Eng. J.*, 2017, **328**, 11–24.
- 34 S. Ncube, P. Kunene, N. T. Tavengwa, H. Tutu, H. Richards, *et al.*, Synthesis and characterization of a molecularly imprinted polymer for the isolation of the 16 US-EPA priority polycyclic aromatic hydrocarbons (PAHs) in solution, *J. Environ. Manage.*, 2017, **199**, 192–200.
- 35 R. Naderi, M. Fedel, F. Deflorian, M. Poelman and M. Olivier, Synergistic effect of clay nanoparticles and cerium component on the corrosion behavior of eco-friendly silane sol–gel layer applied on pure aluminum, *Surf. Coat. Technol.*, 2013, **224**, 93–100.
- 36 C. Y. Lu, T. K. A. Hoang, T. N. L. Doan, M. Acton, H. Zhao, W. S. Guan and P. Chen, Influence of different silica gelling agents on the performance of aqueous gel electrolytes, *J. Ind. Eng. Chem.*, 2016, **42**, 101–106.
- 37 X. X. Liu, P. F. Du, L. Liu, Z. Zheng, X. L. Wang, T. Joncheray and Y. F. Zhang, Kinetic study of Diels–Alder reaction involving in maleimide–furan compounds and linear polyurethane, *Polym. Bull.*, 2013, **70**, 2319–2335.
- 38 H. L. Wei, Z. Yang, H. J. Chu, J. Zhu, Z. C. Li and J. S. Cui, Facile preparation of poly(*N*-isopropylacrylamide)-based



- hydrogels *via* aqueous Diels–Alder click reaction, *Polymer*, 2010, **51**, 1694–1702.
- 39 G. P. Gonzalez, P. F. Hernando and J. S. Durand Alegría, A morphological study of molecularly imprinted polymers using the scanning electron microscope, *Anal. Chim. Acta*, 2006, **557**, 179–183.
 - 40 V. Froidevaux, M. Borne, E. Laborbe, R. Auvergne, A. Gandini and B. Boutevin, Study of the Diels–Alder and retro-Diels–Alder reaction between furan derivatives and maleimide for the creation of new materials, *RSC Adv.*, 2015, **5**, 37742–37754.
 - 41 C. Jegat and N. Mignard, Effect of the polymer matrix on the thermal behaviour of a furan-maleimide type adduct in the molten state, *Polym. Bull.*, 2008, **60**, 799–808.
 - 42 J. Canadell, H. Fischer, G. De With and R. A. T. M. van Benthem, Stereo isomeric effects in thermo-remendable polymer networks based on Diels–Alder crosslink reactions, *J. Polym. Sci., Part A: Polym. Chem.*, 2010, **48**, 3456–3467.
 - 43 A. R. Koohpaei, S. J. Shahtaheri, M. R. Ganjali, *et al.*, Application of multivariate analysis to the screening of molecularly imprinted polymers (MIPs) for ametryn, *Talanta*, 2008, **75**, 978–986.
 - 44 F. L. Wang, M. A. Wang, D. Song, Y. Xu and D. H. Huang, Synthesis of Water Soluble Block Copolymer with temperature and chemical dual-stimuli responsive and its application in renewable heavy metal ion adsorbent, *J. Polym. Mater.*, 2017, **34**, 605–620.
 - 45 D. H. Yang, C. S. Lee, B. H. Jeon, S. M. Choi, Y. D. Kim, J. S. Shin and H. Kim, An electrochemical nanofilm sensor for determination of 1-hydroxypyrene using molecularly imprinted receptors, *J. Ind. Eng. Chem.*, 2017, **51**, 106–112.

